



Towards Biophysical Network Simulation of Stochastically-Formed Neurospheres

Michael J. Bennington¹ and Victoria A. Webster-Wood^{1,2,3,4}

¹ Department of Mechanical, Carnegie Mellon University, Pittsburgh, PA, USA

² Department of Biomedical Engineering, Carnegie Mellon University, Pittsburgh, PA, USA

³ McGowan Institute for Regenerative Medicine, Carnegie Mellon University, Pittsburgh, PA, USA

⁴ Robotics Institute, Carnegie Mellon University, Pittsburgh, PA, USA
vwebster@andrew.cmu.edu

Abstract. Biocomputing platforms, such as cultured neurospheres, have the potential to provide great advances in biohybrid computation and control systems. However, to design and fabricate neurospheres reliably and reproducibly, models that can accurately predict their computational behaviors are required. Towards the end of understanding how neurospheres perform higher-level computations, we present a model framework for simulating the dynamics of stochastically-connected neuron networks. Each neuron is modeled using biophysical models of neural excitability, and the system can be stimulated by a small number of simulated electrodes. The network response of the system is analyzed using Principal Components Analysis on the firing frequencies of the neurons. From preliminary simulations, we demonstrate the ability of these neurosphere networks to encode information about the magnitude of current stimuli. Future additions to this framework will incorporate the 3D geometry of both the neurosphere and individual dendritic trees.

Keywords: Neurospheres · Computational Modeling · Biophysics

1 Introduction

Neurospheres (spherical 3D cultures of neurons and other cells of the nervous systems [33, 43]) and other neuron-based biocomputing platforms present great potential for next-generation computational tools. They can harness the natural capabilities of neural tissue to learn, adapt, and respond to environmental cues. Compared to other state-of-the-art machine learning and artificial intelligence systems, neurospheres operate using a fraction of the energy input, allowing for far more energy-efficient computing [17]. Current state-of-the-art systems have

This material is based on work supported by the National Science Foundation Graduate Research Fellowship under grant No. DGE1745016 and by the NSF Faculty Early Career Development Program under Grant No. ECCS-2044785.

already demonstrated the ability to control robotic systems [8, 39, 41], play simple video games [8, 21], and perform recognition and prediction tasks [7, 8, 34]. Additionally, these neurospheres can serve as organic controllers for muscle-powered biohybrid systems, providing more naturalistic stimulation to the muscles, which has been shown to prolong performance [40].

However, these current systems rely on black-box approaches to tasks, relying on the ability to train neural systems to perform specific actions. If we hope to reliably and robustly design neurosphere systems to perform specific tasks, we must investigate how these systems encode and transform information and how the base units interact. In the case of electronic computers, these characteristics are known [4, 24] - digital computers store information as transistor states (bits) and transform information through Boolean arithmetic; analog computers store information as voltages and currents and transform it using electronic circuit components (resistors, capacitors, etc.). Because of this understanding, designing systems to perform arbitrary tasks is tractable. However, in neural systems, the mechanisms by which individual neuron-to-neuron communication (in the form of temporal- or rate-coded messages) translates to the abstracted latent encodings observed in large neural systems remains unknown [22, 25]. These questions could be investigated using appropriate biophysical simulations of these neurosphere systems.

Existing neurosphere models often focus on the self-organization of the system or the growth and change of these systems [28, 33, 43], related to using these neurospheres as disease models. Fewer models of neural cultures focus on modeling the electrical and computational aspects of these systems or do not model down to the neuron level, rather utilizing lumped approximations for many neurons [27], or other abstracted representations of neural computation, like reservoir computation models [15]. While useful in investigating higher-level dynamics in these systems [12, 15], these abstracted models do not allow us to map these emergent phenomena to the properties at the cellular level as is needed to design computational systems built using living neurons. However, many models exist for modeling the biophysics of neural excitability [6, 13, 20, 26, 29, 35]. By combining these biophysical models of excitability with models of formation and development, we can begin to understand how these neurosphere systems perform computations and how these computations can be designed into systems during formation and during training. In this work, we begin to establish a framework for modeling the electrical activity of stochastically generated neurosphere networks. We combine single-compartment Hodgkin-Huxley models of neuron excitability with a simplified model of stochastic network formation. Preliminary simulations were conducted on networks of various sizes to test the ability of these networks to encode information about input stimuli.

2 Methods

Biophysical simulations of stochastically generated networks were conducted to simulate the behavior of these neurosphere systems. Three neuron types - fast-spiking, regular spiking, and intrinsically bursting neurons - were connected in

networks using both chemical and electrical synapses. The dynamics of each neuron type are modeled as a one-compartment Hodgkin-Huxley system with the ion channels varying between the cell types. An algorithm is developed to stochastically form network connections based on the spatial location of the neurons within the simulated neurosphere.

2.1 Biophysical Neuron Model

The governing dynamics of all three neuron types take the form of a single-compartment Hodgkin-Huxley system. Each cell type is differentiated by the ion channels present and the parameters of the equivalent circuit components. The form of the Hodgkin-Huxley dynamics for the different cell types are taken from [13, 29] (Eq. 1, Table 1). Briefly, the bilayer of the cell membrane acts as a capacitor, and the various ion channels act as dynamical, voltage-dependent resistors. Voltage sources in series with the ion channels model the electrochemical potential for the corresponding ion species. Finally, chemical and electrical synapses and stimulating electrodes can inject current into the compartment. Additionally, in our framework, we add background noisy currents [18].

The governing circuit equation for the compartment takes the form:

$$C_m \frac{dV}{dt} = I_{chem.}(t) + I_{elec.}(t) + I_{noise}(t) - \sum_c (\hat{g}_c A_c(t, V)(V(t) - E_c)) \quad (1)$$

where C_m and V are the membrane capacitance per unit surface area and the membrane voltage, $I_{chem.}$, $I_{elec.}$, and I_{noise} are the cumulative chemical and electrical synapse currents and noise currents, and the summation term represents the total ion channel currents. The form of the chemical and electrical synaptic currents are discussed in Sect. 2.2. The noise current is modeled as a piecewise-constant current source with duration τ_{noise} and magnitude sampled from a mean-zero normal distribution with standard deviation $2\sigma_{noise}$. The window width τ_{noise} is the reciprocal of the highest noise frequency.

The ion channels that are included in the summation term depend on the neuron type in question. For fast-spiking neurons, only two ion channels are present. These are fast-inactivating sodium ion channels and fast-activating potassium channels. These two channels are sufficient for generating action potentials. For regular spiking neurons, an additional slow potassium current is added. This allows the firing frequency of the regular neurons to adapt over time to a constant stimulus. A calcium ion channel is also present for the intrinsically bursting neurons, which allows for rapid bursting at the onset of stimulation, followed by slower spiking. Finally, all neurons contain a non-voltage-dependent leaky ion channel. For this channel, $A_c(t, V) = 1$. Representative single-neuron voltage traces for these cell types are shown in Fig. 1 for a 200 ms constant current stimulation.

For the ion channel c , \hat{g}_c is the maximal conductance per unit surface area, $A_c(t, V)$ is the dynamical, voltage-dependent level of activation, and E_c is the electrochemical potential. The form that $A_c(t, V)$ takes depends on the ion channel, and the specific forms are found in Table 1. For all ion channels in this model,

the activation function will consist of the product of gating variables [13]. The dynamics of these gating variables take the form:

$$\frac{dx}{dt} = \alpha_x(V)(1 - x) + \beta_x(V)x \quad (2)$$

where the specific forms of $\alpha_x(V)$ and $\beta_x(V)$ for the different gating variables are found in Table 1. This is true for all gating variables except for the gating variable for slow potassium currents, which follows dynamics characterized by:

$$\frac{dp}{dt} = \frac{p_\infty(V) - p}{\tau_p(V)} \quad (3)$$

(see also Table 1 for the forms of $p_\infty(V)$ and $\tau_p(V)$). All parameters used in the present simulations are summarized in Table 2 in the Appendix.

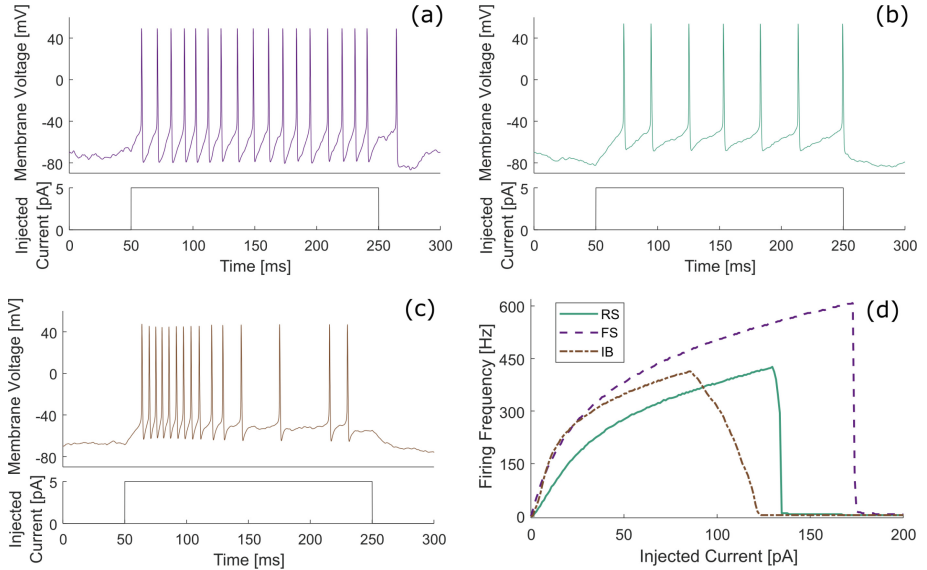


Fig. 1. Behavior of Different Neuron Types. (a)–(c) Representative simulation of each neuron type subjected to a 200 ms constant current injection of 5 pA. (a) Fast-spiking (FS) neuron. (b) Regular spiking (RS) neuron. (c) Intrinsically bursting (IB) neuron. Each neuron was also subject to a noise current with parameters $\tau_{noise} = 1$ ms and $\sigma_{noise} = 1$ pA. This noise current is responsible for the spike that occurs in the FS neuron after the deactivation of the current injection. (d) Frequency-current curves for the different neuron types. Each neuron type was subjected to a 300 ms constant current stimulation, and the average firing frequency across the full stimulation duration was calculated. No noise current was included in these simulations.

Finally, the parameters in the circuit equation are normalized per unit membrane surface area. To obtain the non-normalized values of the parameters, a

Table 1. Ion Channel Gating Dynamics. Here, V_T controls the threshold voltage of the neuron, and τ_{max} is the maximum time constant of the slow potassium ion channel. All gating variables are dimensionless and in the range [0, 1].

Ion Channel	Activation Function	Gating Variable	$\alpha(V)$	$\beta(V)$
Fast-Inactivating Sodium	$A_{Na} = m^3 h$	m	$\frac{-0.32(V - V_T - 13)}{e^{-(V-V_T-13)/4} - 1}$	$\frac{0.28(V - V_T - 40)}{e^{(V-V_T-40)/5} - 1}$
		h	$0.128e^{-(V-V_T-17)/18}$	$\frac{4}{e^{-(V-V_T-40)/5} + 1}$
Fast-Activating Potassium	$A_K = n^4$	n	$\frac{-0.032(V - V_T - 15)}{e^{-(V-V_T-15)/5} - 1}$	$0.5e^{-(V-V_T-10)/40}$
Calcium	$A_{Ca} = q^2 s$	q	$\frac{-0.055(V + 27)}{e^{-(V+27)/3.8} - 1}$	$0.94e^{-(V+75)/17}$
		s	$0.000457e^{-(V+13)/50}$	$\frac{0.0065}{e^{-(V+15)/28} + 1}$
			$p_\infty(V)$	$\tau_p(V)$
Slow-Activating Potassium	$A_K^{slow} = p$	p	$\frac{1}{e^{-(V+35)/10} + 1}$	$\frac{\tau_{max}}{3.3e^{(V+35)/20} + e^{-(V+35)/20}}$

geometry for the neuron compartments is required. As a first-order approximation, here it is assumed that the dynamics are predominantly governed by the axon initial segment (AIS), where it has been shown that the post-synaptic currents are integrated and the actional potential is initiated [1, 14, 32]. For all neuron types, it is assumed that the AIS is approximately a cylinder with a diameter of 3 μm and a length of 30 μm [32].

2.2 Electrical and Chemical Synapse Model

The neurons in the neurosphere network can be connected by either chemical or electrical synapses (or both). Electrical synapses allow for bidirectional current exchange between the neurons, whereas chemical synapses only allow unidirectional currents. The synapse model utilized here is adopted from [13, 16]. For electrical synapses, the current from pre-synaptic neuron j to post-synaptic neuron i takes the form:

$$I_{ij} = g_{ij}^e (V_j(t) - V_i(t)) \quad (4)$$

where g_{ij}^e is the synaptic strength (units: mS) between the two neurons. Because of the bi-directionality of the synapse, $I_{ij} = -I_{ji}$. For chemical synapses, the current from pre-synaptic neuron j to post-synaptic neuron i takes the form:

$$I_{ij} = g_{ij}^c r_j(t) (V_{syn}^j - V_i(t)) \quad (5)$$

where g_{ij}^c is the synaptic strength (units: mS), V_{syn} is the synaptic reversal potential, and r_j is the level of activation, modeling the fraction of bound neurotransmitter receptors. The dynamics of the receptor follow the kinetic equation:

$$\frac{dr_j}{dt} = \left(\frac{1}{\tau_r} - \frac{1}{\tau_d} \right) \frac{1 - r_j}{1 + e^{-V_j + V_0}} - \frac{1}{\tau_d} r_j \quad (6)$$

where τ_r and τ_d are the rise and decay time constants of the synapse, and V_0 is related to voltage at which the concentration of neurotransmitters reaches half of its maximal value [10]. All parameters related to the chemical synapses are summarized in Table 2.

2.3 Stochastic Network Formation

To model the formation of synaptic connection taking place in neurosphere cultures, stochastically-formed networks of the above-mentioned neuron types are constructed using the following process (summarized in Fig. 2):

First, a population of neurons, N , is drawn from a user-specified population prior using a Roulette Sampling technique [42]. Here, N is the user-specified number of neurons in the network. These neurons are placed in 2D space using a noisy sunflower seed pattern [38]. For neuron i , its position in polar coordinates is determined as:

$$[r_i, \theta_i] = \left[\sqrt{\frac{i}{N}}, \frac{2\pi}{\phi^2} i \right] \quad (7)$$

where $\phi = (1/2)(1+\sqrt{5})$ is the golden ratio. The Cartesian position of the neuron is then

$$[x_i, y_i]^T = [r_i \cos(\theta_i) + \xi_x, r_i \sin(\theta_i) + \xi_y]^T \quad (8)$$

where ξ_j is uniformly distributed random variable on the interval $[-0.01, 0.01]$, or 1% of the network size. Note that here the units of the 2D space are not considered. Without geometric consideration in the circuit model, it is not meaningful to prescribe dimensional geometry to the network.

With the neuron positioned in 2D space, we turn next to the formation of synaptic connections. For neuron i , the formation of its dendritic tree takes two steps. First, an axon projects in a randomly chosen direction. This direction is sampled from a normal distribution centered on the inverse-distance-weighted direction $\bar{\mathbf{n}}_i$ from neuron i to all other neurons in the network, calculated as:

$$\bar{\mathbf{n}}_i = \frac{\sum_j \frac{1}{|\mathbf{x}_j - \mathbf{x}_i|} \hat{\mathbf{n}}_{ij}}{\sum_j \frac{1}{|\mathbf{x}_j - \mathbf{x}_i|}} \quad (9)$$

where $\hat{\mathbf{n}}_{ij}$ is the unit vector from neuron i to neuron j . The standard deviation of the distribution is a user-specific parameter and defines the spread of the model “growth cone.” This process takes inspiration from how neurons grow in response to chemical cues from other neurons and how the concentration of those cues will decay with distance [31, 36]. However, this model requires future validation in

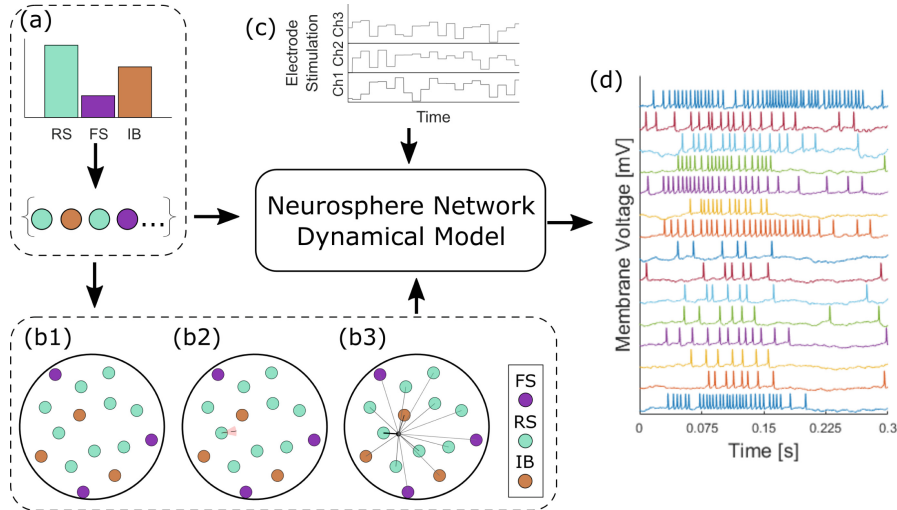


Fig. 2. Stochastic Neurosphere Network Framework. Here, the algorithm used to create and simulate neurosphere networks is summarized for a 15-neuron network. (a) Neuron types (see legend for color) are randomly sampled using user-specified prior and (b1) distributed in 2D space in a noisy sunflower-seed pattern. (b2) Direction of axonal growth is randomly sampled from a Gaussian distribution (red region shows $\pm 2\sigma$) centered on the inverse-distance-weight average direction to neighboring neurons. (b3) With the axon direction chosen (dark line), a branch location is specified (black dot). Connections are randomly made from the branch point to neighboring neurons, with the probability being proportional to the inverse distance to the branch point. The darkness of lines is proportional to the probability of synaptic formation. (c) To investigate neurosphere dynamics, randomly generated, piecewise-constant current stimulation is provided to three input neurons. The resulting membrane voltage of all neurons in the neurosphere is then calculated (d).

the context of 3D culture, as these previous works observed or modeled growth in planar culture. Next, the axon is projected a fixed distance¹ in the direction sampled above, and a branching point is placed at the end of the axon. Connections from neuron i to other neurons will originate at this branching point. To determine how many presynaptic connections neuron i will make with other neurons, a random integer m_{con} is sampled from the interval $[1, M_{con}]$, where $M_{con}(N)$ is the user-specified maximal number of presynaptic connections that a neuron can make based on the number of other neurons present. Then, neu-

¹ The distance of the pre-branching axon projection was chosen to be less than the typical spacing of neurons in the 2D model geometry. This would prevent neurons from intersecting. However, as mentioned above, there are no physical units for the system geometry, including this distance. This parameter can also be tuned in the future to better reflect a typical branching distance observed in neurons. In terms of the model units chosen for the graphical representation of the network, this distance was set to 50 model units.

rons in the network were randomly sampled (with replacement) again using a Roulette Sampling technique until a set of synaptic connections of size m_{con} was constructed. Here, the probability of forming a synapse between two neurons is proportional to the inverse distance between them. Each synapse formed between two neurons is randomly assigned to be either chemical or electrical via Roulette Sampling of a user-specified prior, and the synaptic strength is set to a fixed increment $\Delta g^j (j \in [\text{chemical, electrical}])$. If a duplicate synapse is formed between two neurons (e.g., a new chemical synapse is added where one already exists), the synaptic strength is simply increased by Δg^j .

The functional form of $M_{con}(N)$ was chosen to reflect the observation that neurons in 2D cultures tend to form fewer synapses per neuron in higher-density cultures [9]. For simplicity in these preliminary investigations, the following model was chosen:

$$M_{con}(N) = \text{round} \left(100 \left(1 - \frac{N}{100} \right) \right) \quad (10)$$

However, in 2D neuron cultures, nonlinear relationships were observed [9], so the exact functional form should be further refined based on experimental measurements in 3D neurosphere cultures. Additionally, in its current form, this model is only meaningful for neurospheres of less than 100 neurons, as after this point, the number of connections would be negative. An updated model would be required for larger neurospheres. Similarly, it has also been observed that in higher-density cultures, the conductivity of synapses also decreases, seen as smaller post-synaptic potentials for the same stimulation [19]. As with the M_{con} , a simplified model is utilized here and requires further calibration for 3D neurosphere cultures. Specifically, the increment in synaptic conductivity is modeled as:

$$\Delta g^j(N) = (1 \times 10^{-8}) \left(1 - \frac{N}{100} \right) \text{ mS} \quad (11)$$

The same functional form was used for chemical and electrical synapses. As mentioned for the model for M_{con} , this is limited to the case of less than 100 neurons and needs refinement informed by experimental measures.

2.4 Computational Experiments

To investigate the dynamics of these neurosphere networks, simulations were conducted with randomly generated input stimuli. Three neurons served as inputs to the system, those neurons being the ones located closest to the north-, west-, and south-most regions of the network. These neurons received trains of 60 ms current pulses, whose amplitude was sampled from a uniform distribution on the interval [0,20 pA].

Membrane voltage traces from simulated experiments were used to obtain spiking information from the neurosphere. To determine if a spike occurred, local peaks in the membrane voltage trace were identified using the MATLAB *findpeaks* function (MATLAB r2022b, MathWorks). To avoid obtaining false

spikes due to subthreshold noise, a minimum voltage value for the peaks was set at 20 mV. From this spike train, an instantaneous firing frequency was calculated based on the number of spikes that occur in half-overlapping windows of width 20 ms. This window size was small enough that multiple samples could be taken within a single stimulation pulse. The instantaneous firing frequency was then smoothed with a 5-point moving average filter (*smooth*, MATLAB r2022b, MathWorks), giving a continuous firing frequency response for the neuron. This same analysis was conducted for all neurons in the neurosphere.

As a first step towards investigating possible latent encodings that are captured in these neurosphere networks, principal components analysis was performed on these firing frequency data. The value of the continuous firing frequency response was sampled in the same half-overlapping windows as above. From the time series firing frequency data for all neurons, the principal component axes and corresponding data projects were calculated (*pca*, MATLAB r2022b, MathWorks). The first three principal components were selected for further analysis. This number was chosen both to allow for graphical investigation and because it was observed that the amount of variance contained in subsequent components decayed rapidly. However, the number of information-containing components will likely change with the scale of the neurosphere and warrants its own investigation beyond the scope of this work.

2.5 Numerical Implementation

The present model was implemented using a custom MATLAB library. All simulations were solved using a variable-order, variable-step stiff differential equations solver (*ode15s*, MATLAB r2022b, MathWorks). For the present study, all simulations were conducted using an AMD Ryzen 5 5600X 6-core processor (3.70 GHz, 16 GB RAM). For the sake of reproducibility, all simulations were conducted starting with the same seed value for the MATLAB pseudorandom number generator of 200000 at the beginning of network formation. All code will be provided upon request. The current implementation of the solver scheme has not been optimized, as this was beyond the scope of this work. However, we plan to optimize for computational speed during the future development of this tool.

3 Results and Discussion

Using the proposed model framework, example simulations were conducted for networks of size $N = [15, 30, 45]$ (Fig. 3). Each simulation was run for 100 stimulation epochs, with a max stimulation current of 20 pA, and noise parameters $\sigma_{noise} = 5$ pA and $\tau_{noise} = 1$ ms. From the resulting time series membrane voltages (Fig. 4(a1–c1)), firing frequency was calculated, and principal components analysis was conducted on the firing frequency in fixed-width time bins. The first three principal components were considered for additional graphical analysis (Fig. 4(a2–c2)). These components covered 75.8%, 65.5%, and 44.2% of the variance for the $N = 15$, $N = 30$, and $N = 45$ cases, respectively.

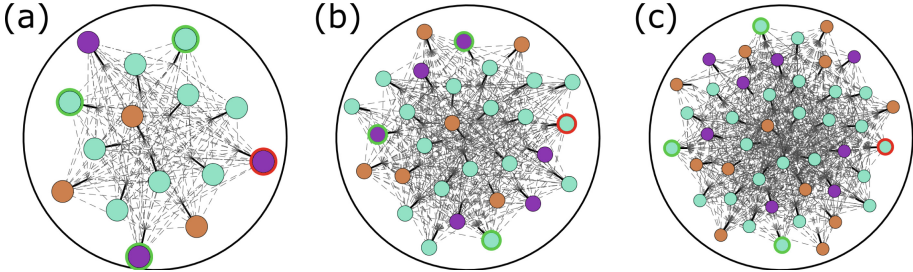


Fig. 3. Example Neurosphere Formation Network structures for size (a) $N = 15$, (b) $N = 30$, (c) $N = 45$. Colors correspond to the same neuron types as in Fig. 2, and the line style between two neurons showing the type of connection (dashed: chemical synapse only, dotted: electrical synapse only, dot-dashed: both electrical and chemical synapses). Green highlighting indicates the input neuron, and red highlighting indicates the output neuron. (Color figure online)

From a qualitative analysis of the membrane voltage time series, smaller networks showed higher firing frequencies with greater degrees of synchronicity between groups of neurons. Conversely, in larger networks, each individual neuron tended to show lower firing frequencies. This will be related to the choice of density-dependent maximum connectivity and synaptic conductivity increment. Additionally, observing the principal components of the firing frequencies, there appear to be input-current-related groupings (Fig. 4(a2–c2)). In these figures, the RGB values of the data point colors correspond to the stimulation current magnitude on input channels 1, 2, and 3, respectively. The input current-related groupings can be observed as clusters of similarly colored dots. This becomes more apparent in larger networks, where these groupings have more well-defined boundaries compared to the smaller networks. This suggests it is possible to encode input stimulus information in the firing frequency of these randomly connected networks. Further work is needed, however, to investigate the mapping between input and latent states, as well as the robustness of these encodings to stochasticity in the network. Additionally, it was observed that in the larger networks, more principal components contained a sizeable amount of the variance. Therefore, more components may need to be considered in these larger networks than the three that can be readily visualized.

The present model framework allows for preliminary simulations of neurosphere-like systems. However, multiple aspects require further refinement before it can be used as a predictive design tool. The first area of improvement concerns the system's lack of relevant geometry. Currently, neurons act as point compartments in dimensionless 2D space. In true neurospheres and neural systems in general, neurons have sprawling geometries that extend in all three dimensions [2]. This venture into the third dimension increases the degrees of freedom the neurons have to form synaptic connections. Additionally, this geometry means that neurons are not single components but consist of branching trees of axons and dendrites, the lengths and geometries of which contribute

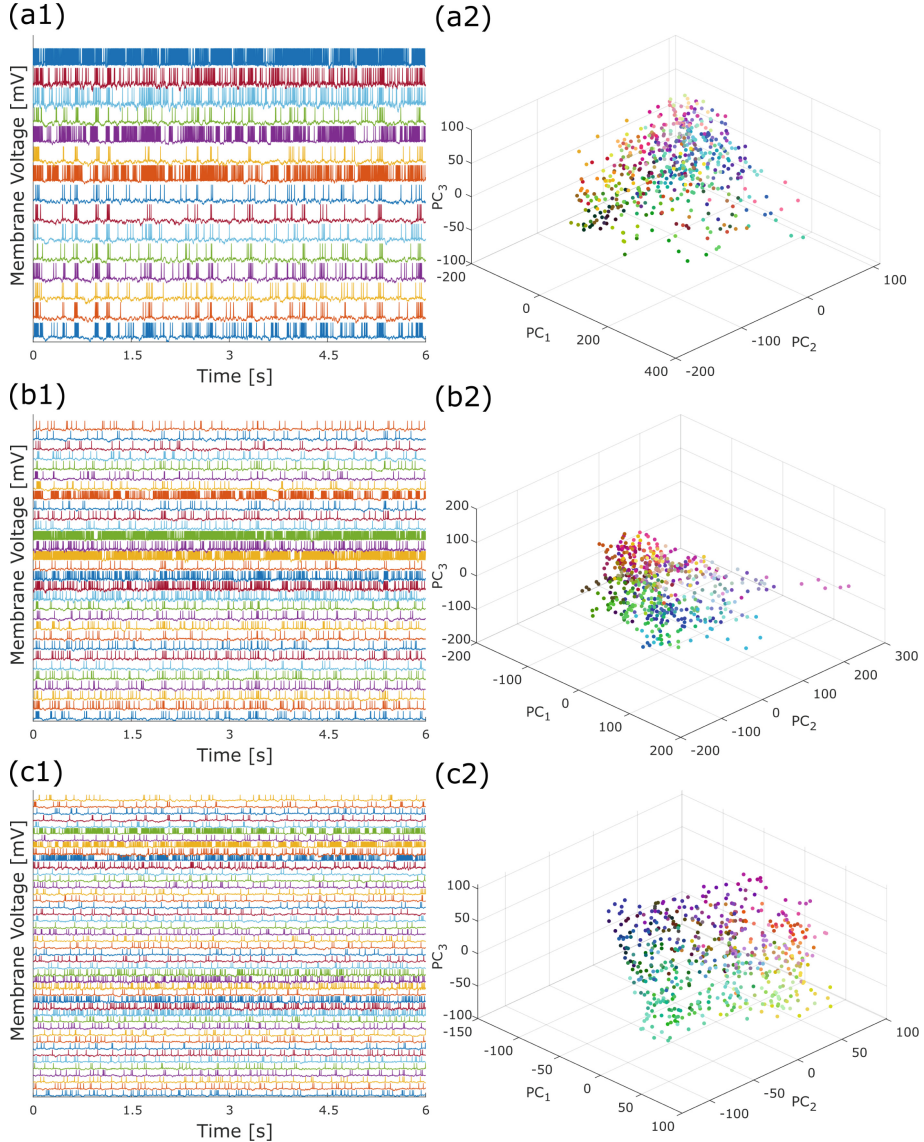


Fig. 4. Network Simulation Results. (a1–c1) Membrane voltage traces for the networks shown in Fig. 3. (a2–c2) Structure of first three principal components. The color of each dot corresponds to the input stimulus, with the red, green, and blue components corresponding to the normalized current magnitude on input channels 1, 2, and 3, respectively. (Color figure online)

to time delays in signal transmission [30] and other emergent electrical properties [11, 23, 37]. For more accurate modeling of these systems, these geometry-dependent effects should be incorporated either directly by incorporating mul-

ticompartiment models of the axon and dendrites [3] or time-delay differential equations [5] for the synaptic connections. Finally, the spacing of neurons in the neurospheres will also be impacted by the volume fraction of non-neuronal cells in the culture. For smaller neuronal volume fractions, neurons will be, on average, farther apart from each other, changing their likelihood of connecting and the connection strength. This volume fraction and the stochastic arrangement of cells in packed 3D space could also be incorporated [33, 43].

The second area of improvement required for the model relates to the specific choice of sampling priors and parameter relationships. For these initial investigations, simplifications were made in the functional forms relating the maximal connectivity density and incremental synapse conductivity to the seeding density of neurons. The exact functional form can be refined from morphological and electrophysiological investigations of cultured neurospheres. Additionally, the various sampling priors used in this work were not calibrated to data. Finally, the types and parameters of the ion channels used in the circuit models were fixed and taken from the literature. To better reflect the cell sources utilized to build neurospheres, these parameters and their associated population distributions should be measured. These experimental results could be used to refine the model for the specific cell sources used. Finally, additional computational investigation could focus on the network's sensitivity to the different sampling and parameter priors. To maximize the impact of experiments, the parameters that are found to impact the model most could be prioritized. Additionally, if designers were able to customize the priors (using specific cell separation techniques or different mixtures of cell sources), then these sensitivities would allow them to predict the effect of a new prior and to begin optimizing these systems for specific tasks.

4 Conclusion

In this work, we present a model framework for simulating stochastically-formed neuron networks toward understanding the biophysics of neurosphere computation. Individual neurons are modeled using single-compartment Hodgkin-Huxley models with different combinations of ion channels, and we present a novel approach to model the stochastic formation of connections in neurospheres. Using this framework, we conduct preliminary simulations of networks of various sizes. In these simulations, it was observed that the current magnitude of input stimuli could be encoded in the principal components of firing frequencies. Future works will aim to increase the model's realism by incorporating the effects of 3D geometry and to increase the model's specificity through experimental characterization and validation of the constituent elements. This refined model will then be compared to experimentally measured neurosphere spikes trains.

Acknowledgement. The authors would like to thank Drs. Wayne Wu, Alison Barth, Joseph Najem, and Tzahi Cohen-Karni for their stimulating conversations during the formulation of this work.

Appendix

Table 2. Model Parameters. All parameters used in the model are summarized here. Most variables are taken verbatim from [13] and [29]. However, some are modified to better match the qualitative descriptions of the neurons proposed in those papers.

Parameter	Regular Spiking Neurons	Fast Spiking Neurons	Intrinsically Bursting Neurons
Neuron Parameters:			
C_m [$\mu\text{F}/\text{cm}^2$]	1	0.5	1
E_K [mV]		-90	
E_{Na} [mV]	56	50	50
E_{Ca} [mV]	—	—	120
E_L [mV]	-70.3	-70	-70
\hat{g}_K [mS/cm^2]	6	10	10
\hat{g}_{Na} [mS/cm^2]		56	
\hat{g}_{Ca} [mS/cm^2]	—	—	0.2
\hat{g}_K^{slow} [mS/cm^2]	0.075	—	0.075
\hat{g}_L [mS/cm^2]	0.0205	0.015	0.0205
τ_p^{max} [ms]	608	—	608
V_T [mV]		-56.2	
Synapse Parameters:			
τ_r [ms]		0.5	
τ_d [ms]		8	
V_{syn} [mV]	20	-80	20
V_0 [mV]		-20	

References

1. Alcami, P., El Hady, A.: Axonal computations. *Front. Cell. Neurosci.* **13**(September), 1–19 (2019). <https://doi.org/10.3389/fncel.2019.00413>
2. Ascoli, G.A., Donohue, D.E., Halavi, M.: NeuroMorpho.Org: a central resource for neuronal morphologies. *J. Neurosci.* **27**(35), 9247–9251 (2007). <https://doi.org/10.1523/JNEUROSCI.2055-07.2007>

3. Bhalla, U.S.: Multi-compartment models of neurons. In: Computational Systems Neurobiology, vol. 7, pp. 1–570 (2012). <https://doi.org/10.1007/978-94-007-3858-4>
4. Block, F.E.: Analog and digital computer theory. Int. J. Clin. Monit. Comput. **4**(1), 47–51 (1987)
5. Bocharov, G.A., Rihan, F.A.: Numerical modelling in biosciences using delay differential equations. J. Comput. Appl. Math. **125**(1–2), 183–199 (2000). [https://doi.org/10.1016/S0377-0427\(00\)00468-4](https://doi.org/10.1016/S0377-0427(00)00468-4)
6. Burkitt, A.N.: A review of the integrate-and-fire neuron model: I. Homogeneous synaptic input. Biol. Cybern. **95**(1), 1–19 (2006)
7. Cai, H., et al.: Brain organoid reservoir computing for artificial intelligence. Nat. Electron. **6**(12), 1032–1039 (2023). <https://doi.org/10.1038/s41928-023-01069-w>
8. Chen, Z., et al.: An overview of *in vitro* biological neural networks for robot intelligence. Cyborg Bionic Syst. **4** (2023). <https://doi.org/10.34133/cbsystems.0001>
9. Cullen, D.K., Gilroy, M.E., Irons, H.R., Laplaca, M.C.: Synapse-to-neuron ratio is inversely related to neuronal density in mature neuronal cultures. Brain Res. **1359**, 44–55 (2010). <https://doi.org/10.1016/j.brainres.2010.08.058>
10. Destexhe, A., Mainen, Z.F., Sejnowski, T.J.: Models of synaptic transmission. In: Methods in Neuronal Modeling, pp. 1–25 (1998). https://doi.org/10.1007/978-3-642-46345-7_11
11. van Elburg, R.A., van Ooyen, A.: Impact of dendritic size and dendritic topology on burst firing in pyramidal cells. PLoS Comput. Biol. **6**(5), 1–19 (2010). <https://doi.org/10.1371/journal.pcbi.1000781>
12. Enel, P., Procyk, E., Quilodran, R., Dominey, P.F.: Reservoir computing properties of neural dynamics in prefrontal cortex. PLoS Comput. Biol. **12**(6), 1–35 (2016). <https://doi.org/10.1371/journal.pcbi.1004967>
13. Giannari, A.G., Astolfi, A.: Model design for networks of heterogeneous Hodgkin-Huxley neurons. Neurocomputing **496**, 147–157 (2022). <https://doi.org/10.1016/j.neucom.2022.04.115>
14. Goethals, S., Brette, R.: Theoretical relation between axon initial segment geometry and excitability. eLife **9**, 1–34 (2020). <https://doi.org/10.7554/eLife.53432>
15. Gürel, T., Rotter, S., Egert, U.: Functional identification of biological neural networks using reservoir adaptation for point processes. J. Comput. Neurosci. **29**(1–2), 279–299 (2010). <https://doi.org/10.1007/s10827-009-0176-0>
16. Hao, Y., Gong, Y., Wang, L., Ma, X., Yang, C.: Single or multiple synchronization transitions in scale-free neuronal networks with electrical or chemical coupling. Chaos, Solitons Fractals **44**(4–5), 260–268 (2011). <https://doi.org/10.1016/j.chaos.2011.02.005>
17. Howarth, C., Gleeson, P., Attwell, D.: Updated energy budgets for neural computation in the neocortex and cerebellum. J. Cereb. Blood Flow Metab. **32**(7), 1222–1232 (2012). <https://doi.org/10.1038/jcbfm.2012.35>
18. Huber, M.T., Braun, H.A.: Conductance versus current noise in a neuronal model for noisy subthreshold oscillations and related spike generation. Biosystems **89**(1–3), 38–43 (2007). <https://doi.org/10.1016/j.biosystems.2006.05.009>
19. Ivenshitz, M., Segal, M.: Neuronal density determines network connectivity and spontaneous activity in cultured hippocampus. J. Neurophysiol. **104**(2), 1052–1060 (2010). <https://doi.org/10.1152/jn.00914.2009>
20. Izhikevich, E.M.: Simple model of spiking neurons. IEEE Trans. Neural Netw. **14**(6), 1569–1572 (2003). <https://doi.org/10.1109/TNN.2003.820440>

21. Kagan, B.J., et al.: *In vitro* neurons learn and exhibit sentience when embodied in a simulated game-world. *Neuron* **110**(23), 3952–3969.e8 (2022). <https://doi.org/10.1016/j.neuron.2022.09.001>
22. Koren, V., Bondanelli, G., Panzeri, S.: Computational methods to study information processing in neural circuits. *Comput. Struct. Biotechnol. J.* **21**, 910–922 (2023) <https://doi.org/10.1016/j.csbj.2023.01.009>. <https://www.sciencedirect.com/science/article/pii/S2001037023000119>
23. Krichmar, J.L., Nasuto, S.J., Scorcioni, R., Washington, S.D., Ascoli, G.A.: Effects of dendritic morphology on CA3 pyramidal cell electrophysiology: a simulation study. *Brain Res.* **941**(1–2), 11–28 (2002). [https://doi.org/10.1016/S0006-8993\(02\)02488-5](https://doi.org/10.1016/S0006-8993(02)02488-5)
24. Lewin, D., Noaks, D.: Theory and Design of Digital Computer Systems. Springer, Dordrecht (1992). <https://doi.org/10.1007/978-94-011-1576-6>
25. Libedinsky, C.: Comparing representations and computations in single neurons versus neural networks. *Trends Cogn. Sci.* **27**(6), 517–527 (2023). <https://doi.org/10.1016/j.tics.2023.03.002>. <https://linkinghub.elsevier.com/retrieve/pii/S1364661323000645>
26. Long, L., Fang, G.: A review of biologically plausible neuron models for spiking neural networks. In: AIAA Infotech@Aerospace 2010. American Institute of Aeronautics and Astronautics, Atlanta, Georgia (2010)
27. Massobrio, P., Martinoia, S.: Modelling small-patterned neuronal networks coupled to microelectrode arrays. *J. Neural Eng.* **5**(3), 350–359 (2008). <https://doi.org/10.1088/1741-2560/5/3/008>
28. Poli, D., Magliaro, C., Ahluwalia, A.: Experimental and computational methods for the study of cerebral organoids: a review. *Front. Neurosci.* **13**(March), 1–13 (2019). <https://doi.org/10.3389/fnins.2019.00162>
29. Pospischil, M., et al.: Minimal Hodgkin-Huxley type models for different classes of cortical and thalamic neurons. *Biol. Cybern.* **99**(4–5), 427–441 (2008). <https://doi.org/10.1007/s00422-008-0263-8>
30. Puppo, F., George, V., Silva, G.A.: An optimized structure-function design principle underlies efficient signaling dynamics in neurons. *Sci. Rep.* **8**(1), 1–15 (2018). <https://doi.org/10.1038/s41598-018-28527-2>
31. Qian, K., Liao, A.S., Gu, S., Webster-Wood, V.A., Zhang, Y.J.: Biomimetic IGA neuron growth modeling with neurite morphometric features and CNN-based prediction. *Comput. Methods Appl. Mech. Eng.* **417**, 116213 (2023). <https://doi.org/10.1016/j.cma.2023.116213>
32. Rotterman, T.M., Carrasco, D.I., Housley, S.N., Nardelli, P., Powers, R.K., Cope, T.C.: Axon initial segment geometry in relation to motoneuron excitability. *PLoS ONE* **16**(11) (2021). <https://doi.org/10.1371/journal.pone.0259918>
33. Sipahi, R., Zupanc, G.K.: Stochastic cellular automata model of neurosphere growth: roles of proliferative potential, contact inhibition, cell death, and phagocytosis. *J. Theor. Biol.* **445**, 151–165 (2018). <https://doi.org/10.1016/j.jtbi.2018.02.025>
34. Sumi, T., et al.: Biological neurons act as generalization filters in reservoir computing. *Proc. Natl. Acad. Sci.* (2023). <https://doi.org/10.1073/pnas.2217008120>
35. Szczecinski, N.S., Hunt, A.J., Quinn, R.D.: A functional subnetwork approach to designing synthetic nervous systems that control legged robot locomotion. *Front. Neurorobot.* **11**, 1–19 (2017). <https://doi.org/10.3389/fnbot.2017.00037>
36. Tamariz, E., Varela-Echavarria, A.: The discovery of the growth cone and its influence on the study of axon guidance. *Front. Neuroanat.* **9**(MAY), 1–9 (2015). <https://doi.org/10.3389/fnana.2015.00051>

37. Vetter, P., Roth, A., Häusser, M.: Propagation of action potentials in dendrites depends on dendritic morphology. *J. Neurophysiol.* **85**(2), 926–937 (2001). <https://doi.org/10.1152/jn.2001.85.2.926>
38. Vogel, H.: A better way to construct the sunflower head. *Math. Biosci.* **44**, 179–189 (1979). [https://doi.org/10.1016/0025-5564\(79\)90080-4](https://doi.org/10.1016/0025-5564(79)90080-4)
39. Warwick, K., et al.: Controlling a mobile robot with a biological brain. *Defence Sci. J.* **60**(1), 5–14 (2010). <https://doi.org/10.14429/dsj.60.11>
40. Won, P., Ko, S.H., Majidi, C., Feinberg, A.W., Webster-Wood, V.A.: Biohybrid actuators for soft robotics: challenges in scaling up. *Actuators* **9**(4), 1–11 (2020). <https://doi.org/10.3390/act9040096>
41. Yada, Y., Yasuda, S., Takahashi, H.: Physical reservoir computing with FORCE learning in a living neuronal culture. *Appl. Phys. Lett.* **119**(17) (2021). <https://doi.org/10.1063/5.0064771>
42. Younes, A., Elkamel, A., Areibi, S.: Genetic algorithms in chemical engineering : a tutorial. *World* (2008)
43. Zhdanov, V.P., Kasemo, B.: Simulation of the growth of neurospheres. *Europhys. Lett.* **68**(1), 134–140 (2004). <https://doi.org/10.1209/epl/i2004-10170-1>